Investigations on the influence of adapted metal-based alloys on the process of laser beam melting

Andreas Wimmer, Cara G. Kolb, Mariam Assi, Julien Favre, Andreas Bachmann, Anna Fraczkiewicz, Michael F. Zaeh

INVESTIGATIONS ON THE INFLUENCE OF ADAPTED METAL-BASED ALLOYS ON THE PROCESS OF LASER BEAM MELTING

Paper LAM 303

Andreas Wimmer[1*], Cara G. Kolb[1*], Mariam Assi[2], Julien Favre[2], Andreas Bachmann[1], Anna Fraczkiewicz[2], Michael F. Zaeh[1]

[1] Technical University of Munich, TUM Department of Mechanical Engineering, Institute for Machine Tools and Industrial Management, Boltzmannstr. 15, 85748 Garching, Germany
[2] Mines Saint-Etienne, Université Lyon, CNRS, UMR 5307 LGF, Centre SMS, Departement PMM, F - 42023 Saint-Etienne France

Abstract

Additive Manufacturing (AM) technologies are characterized by complex process interrelations. Consequently, specifically adapted alloys are required to enable a robust building process. In particular, Laser Beam Melting (LBM) is increasingly used for the fabrication of sophisticated functional parts for various applications in numerous industrial sectors, such as automotive and aerospace.

However, process stability and repeatability is a major challenge for industrializing LBM. This paper presents a comprehensive investigation on the influence of AlSi10Mg additives in a 316L stainless steel powder during LBM. A two-stage experimental approach was applied, during which the temperature field around the molten track and the number of spatters during the LBM process were determined by means of high-speed thermographic imaging. Furthermore, the microstructure of the additively manufactured specimens, the modified 316L stainless steel powder, and the respective raw materials were characterized by Scanning Electron Microscopy (SEM).

The experimental study described in this paper aimed to obtain correlations between the additive content (input), the temperature field of the molten track, and the microstructure (outputs). It was found, that the cooling rate decreases with a higher amount of AlSi10Mg in the powder. Furthermore, the microstructure analysis demonstrated an increasing formation of the Body-Centered Cubic (BCC) phase with a higher fraction of AlSi10Mg. The conclusion is that additives in the powder considerably affect important key characteristics of the LBM process.

Keywords: Alloy Design, Laser Beam Melting (LBM), Melt Pool Stability, High-Speed Thermographic Imaging, Additive Manufacturing (AM)

Introduction and State of the Art

LBM allows the fabrication of complex parts with a short lead time and a reduced material waste [1]. Initially employed for rapid prototyping only, LBM recently achieved a sufficient level of maturity for series production. The emergence of new applications for LBM highlighted the need for specific alloys dedicated to these technologies. Currently, companies working on cutting-edge 3D technologies have access to less than 50 commercially available alloys [2]. Most of the commercial grades have been optimized to form a fine, stable and homogeneous microstructure after conventional deformation processing (forging, drawing). In contrast to conventional manufacturing technologies, LBM is characterized by fast periodic heating and cooling, which results in metastable microstructures and the occurrence of defects [3], such as porosities degrading the material strength [4, 5]. In addition, the occurrence of defects near the surface is severely affecting the fatigue lifetime [6]. According to [7, 8], who conducted in-situ X-ray imaging during LBM, the formation of porosities is associated to melt pool instabilities. Therefore, a higher stability of the melt pool presumably results in a reduction of the fraction of porosities and an increase of the specific strength and fatigue resistance.

An approach to improve the melt pool stability is to develop new alloy compositions dedicated specifically to LBM. These alloys must also allow a better control of the microstructure to improve the strength and thus the competitiveness of 3D printed components.

New complex alloys for LBM can be produced by gas atomization of pre-alloyed ingots [9] or directly by mixing elemental powders [10]. The latter was found to be successful even for elements with very different melting temperatures, providing an acceptable chemical homogeneity for mechanical engineering [11]. A convenient method to adjust the composition of an already available commercial powder is to blend it with an additive. The

[*] The authors contributed equally to this work.

selection of such an additive must be done by considering jointly its effect on the melt pool stability, the occurrence of defects, the microstructure, and the mechanical properties. The goal of this study is to highlight the relevant optimization parameters to determine a suitable additive.

The investigation of aluminum additives in a 316L powder composition was chosen for this purpose, since an increased aluminum content gives the alloy an extremely high stability against the formation of stress-induced martensite. This was reported to be relevant for applications where the prevention of hydrogen embrittlement is required [12].

Therefore, the paper demonstrates the influence of aluminum on the melt pool stability, the thermal properties, and the microstructure. The possibility to affect these three essential groups of properties by driving the solidification during the LBM process is shown experimentally. The properties mostly affected by the chemical composition will be highlighted for future works on the alloy design. Finally, the capability to produce duplex microstructures with Face-Centered Cubic (FCC) and Body-Centered Cubic (BCC) phases by LBM will be discussed.

Approach and Theoretical Considerations

The reference material selected for the study was a 316L austenitic steel, because it is one of the most investigated materials for the LBM process. It is a single-phase material, with a suitable combination of strength and ductility. The additive must significantly affect the physical properties of the blended powder during the melting process. Consequently, it must have a different melting temperature and different thermal properties. Additionally, it must be readily available as a commercial powder. This led to the selection of the aluminum alloy AlSi10Mg, which belongs to the 3000 series and is known for its excellent castability. Furthermore, an increased aluminum content gives the alloy an extremely high stability against the formation of stress-induced martensite.

From the addition of aluminum to 316L significant effects were expected on i) the stability of the melt pool, ii) the thermal behavior of the powder bed and of the part, and iii) the phase stability and microstructure.

i) The addition of AlSi10Mg additives most likely affects the surface tension of the melt pool. In the liquid state aluminum has a surface tension that is half of the one of steel. In addition, the variation of the surface tension with the temperature is lower for aluminum [13]. On the one hand, the joint decrease of the surface tension and of its variation with temperature may reduce the Marangoni convection, which most probably stabilizes the melt pool. On the other hand, the low melting and vaporization point may result in the evaporation of aluminum, promoting the formation of a keyhole and porosities.

ii) The addition of aluminum presumably affects the thermal and physical properties of the blended powder and the part. The modification of the physical properties was estimated by studying the variation of properties for commercial steels (data from Granta Design CES Selector database). The database considers 656 steel grades and 32 grades with an aluminum content between 0.05 % and 2 % wt. Compared to the reference material, the following changes in the physical and thermal properties of the blend were assumed:

- A negligible variation of density, latent heat of solidification, thermal expansion coefficient, and of the specific heat capacity
- An average decrease of the thermal conductivity. Compared to carbon steels the thermal conductivity decreases by about 10 % for dual phase steels containing 1 to 2 % aluminum. This presumption is further corroborated by the results from previous studies on the Fe-Al system [14].

iii) The additive may affect the resulting phases after solidification. Aluminum is known for promoting the BCC phase in steels. However, 316L is an austenitic steel with only a FCC phase. The addition of aluminum would affect the stability of FCC and it would result in two-phased duplex structures with an increasing fraction of BCC. The increase of BCC improves the overall strength to the detriment of ductility.

Experimental Investigations

Modification of the powder compositions

For the experimental investigations, powder compositions with a varying proportion of additives (0 %, 1 %, 5 %) were prepared iteratively. 316L powder (MetcoAdd 316L, Oerlikon Metco, Switzerland) served as a basic alloy and AlSi10Mg (EOS, Germany) was used as an additive. Both powder alloys have a particle size distribution of between $20 - 63$ µm, whereby the AlSi10Mg powder contains a larger fraction of small particles.

Figure 1 schematically illustrates the preparation of the respective powder compositions for the experimental LBM studies.

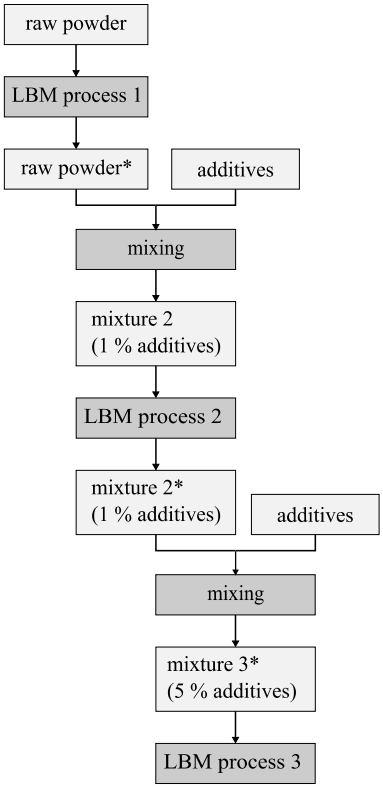

Figure 1: Flow chart showing the preparation of the respective powder compositions for the investigations in LBM.

The first test series (LBM process 1) was conducted with raw 316L powder (raw powder). Subsequently, the powder was removed from the LBM machine (raw powder*) and filled in batches of one kilogram each. The exact weight was determined using a precision balance. The required mass of additives to be added to the respective container to obtain an as-prepared mixture with a mass content of 1 % was calculated according to

$$m_{n+1} = m_n + m_{Add,x} \quad (1)$$

$$m_{Add,x} = m_{Add,n+1} - m_{Add,n} \quad (2)$$

$$m_{Add,x} = \frac{x_{n+1} \cdot m_n - m_{Add,n}}{(1 - x_{n+1})} \quad (3)$$

The powder composition was mixed for 60 s at 750 rpm in a double rotating cylindrical vessel with a diameter of 106 mm (SpeedMixer DAC 3000, Hauschild, Germany) at ambient pressure and temperature to achieve a blended mixture. The homogeneous mixture (mixture 2) was fed into the LBM machine and the second test series was performed (LBM process 2). The described cycle was repeated for the preparation of the powder composition with a mass fraction of 5 % additives. x expresses the targeted additive mass proportion of the mixture to prepare with the mass m_{n+1} on the basis of the previous mixture with the mass m_n. $m_{Add,x}$ stands for the mass of additives, which is required to achieve a composition with a content of x mass-% additives. $m_{Add,n}$ and $m_{Add,n+1}$ describe the actual mass of the additives contained in the mixture n and $n + 1$, respectively.

Investigations of the process during LBM

The LBM experiments were conducted with an EOSINT M270 machine (EOS, Germany). Its front door was modified to allow process monitoring (see Figure 2). For the monitoring, a high-speed thermographic camera (ImageIR 8300, InfraTec, Germany) was used to obtain videos with a high temporal resolution. In order to decrease the working distance of the camera, an inlet was printed via Fused Deposition Modeling (FDM).

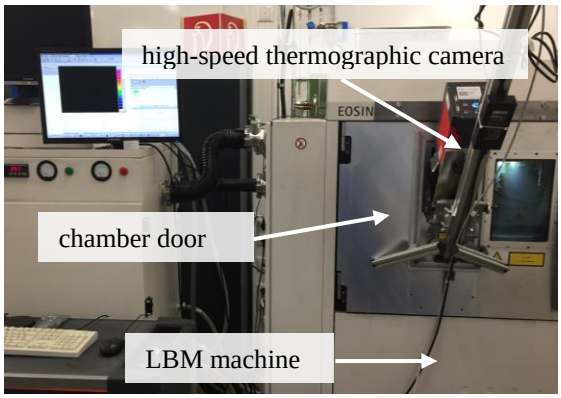

Figure 2: Experimental setup: The door of an EOSINT M270 LBM machine was modified for high-speed thermographic imaging.

The inlet was equipped with a seal for tightness and a protective window (Ge AR-coated, 3 to 12 µm transmission wavelength). The experiments were performed at a constant laser power of P = 175 W, a constant hatch spacing of H = 120 µm and varying scanning speeds of v = 375 mm/s, 500 mm/s and 750 mm/s. Furthermore, the Argon process gas flow was altered by tuning the voltage of the fan with U = 0 V, 1.5 V and 2.5 V.

Microstructure characterization

The material characterization was done by SEM. Electron Back-Scattered Diffraction (EBSD) mapping was conducted on a Zeiss Supra 55 VP microscope operating at 20 kV. The variations of chemical composition were characterized by a Back-Scattered Electron (BSE) detector and by Energy Dispersive X-Ray Spectrometry (EDS) mapping. The identification of phases was achieved by X-Ray Diffraction (XRD) (X'Pert Pro Panalytical) using a Cobalt X-ray tube with a monochromator and an XCelerator detector. The diffraction angle

2θ varied from 45° to 115° with a step size of 0.0376°, and a counting time of 4000 s/step.

Results

Examination of the powder

The morphology of the respective raw materials and powder compositions was examined by SEM (JSM-7500F, Jeol, Germany) (see Figure 3). The images show that the 316L powder without additives contained primarily spherical particles and displays hardly any agglomerates. AlSi10Mg powder exhibited a larger fraction of small particles and a high number of agglomerates. The characteristic properties of the morphology of pure 316L powder and AlSi10Mg powder correlated with the observations of the composition with 5 % additives, respectively. Furthermore, the images indicate that the heat input during mixing did not lead to a presintering of the particles. The results thus confirm that the utilized mixing method is suitable for the preparation of the powder compositions.

Thermographic investigations

During the LBM process, single tracks were recorded with a high-speed thermographic camera. The temperature field of a molten track is depicted in Figure 4 for the investigated powder compositions. The spikes indicate the spatter particles that were expelled from the melt pool. A quantitative analysis of the number of spatter particles showed no significant difference for the three powder compositions.

Due to the highly varying temperatures in the melt pool and the unknown emissivity, it was not feasible to determine absolute temperature values. However, a consideration of the relations between the values was possible. The temperature field was analyzed according to two approaches: firstly at the scale of the seam, to determine the cooling factor during solidification; and secondly on a macroscopic scale to identify the cooling mechanisms.

a) Cooling factor along the seam

A detailed analysis of the temperature in the x-direction is depicted in Figure 5. The experimental data was fitted with Newton's law of cooling:

$$T(x) = T_s + (T_b - T_s) \cdot e^{-f \cdot x} \qquad (4)$$

with the surrounding temperature T_s, beginning temperature T_b, and the cooling factor f.

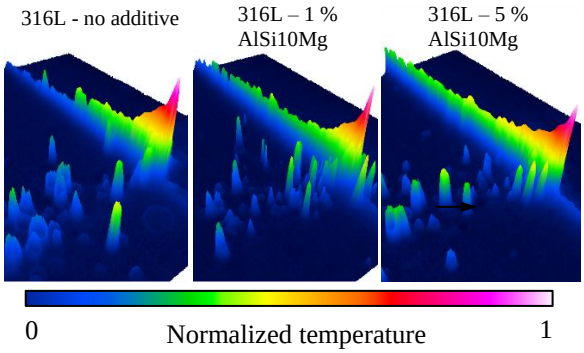

Figure 4: Three dimensional illustration of a track for v = 375 mm/s and U = 1.5 V. The spikes indicate the spatter particles.

The qualitative observation of Figure 4 regarding the surrounding temperature was confirmed by the fitted model: The higher the amount of AlSi10Mg, the higher was the surrounding temperature. This finding is directly related to the temperature gradient that is responsible for various effects in LBM, e.g. residual stresses and deformations. Furthermore, a dependency became obvious between the amount of added AlSi10Mg and the cooling factor (see Table 1).

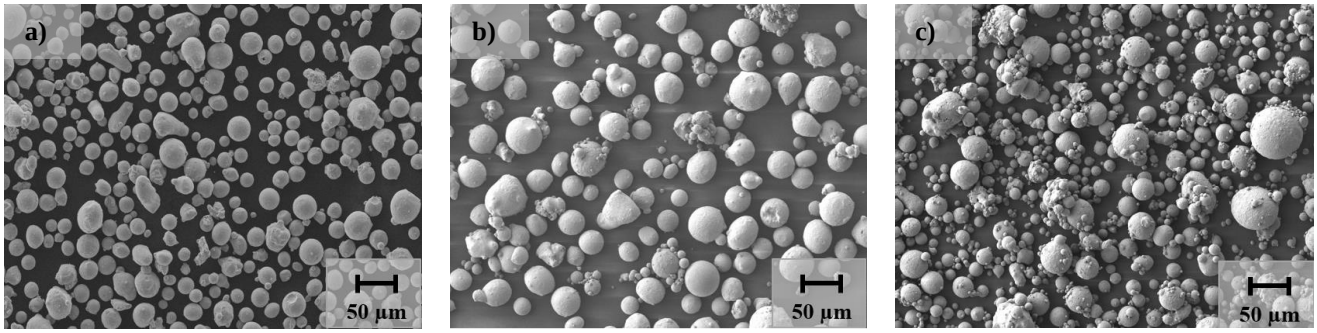

Figure 3: SEM images of relevant powder compositions with a) 316L – no additive b) 316L – 5 % AlSi10Mg c) AlSi10Mg (acceleration voltage: 1.0 kV, signal type SE).

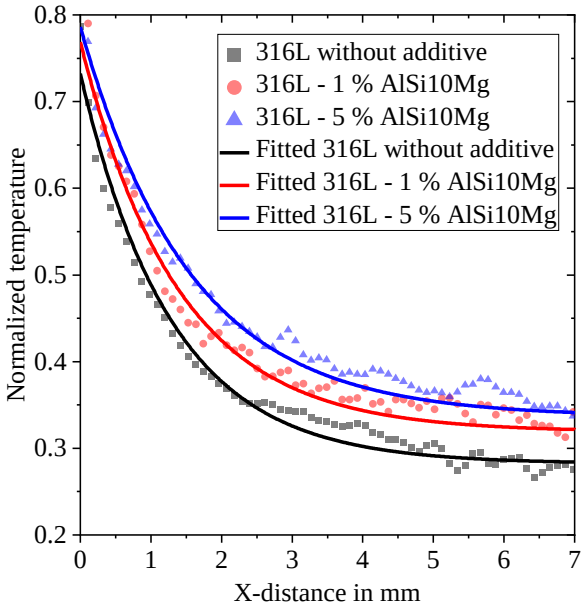

Figure 5: Temperature values in x-direction. The solid lines indicate the fitted Newton's law of cooling.

Table 1: Fit values of Figure 5 (f according to Equation 4).

	316L – no additive	**316L – 1 % AlSi10Mg**	**316L – 5 % AlSi10Mg**
Adj. R^2	0.95	0.97	0.98
***f* in 1/mm**	0.35±0.008	0.33±0.008	0.29±0.006

b) Modeling of the thermal field

The 2D thermal field at the surface of the powder bed can be modelled using the Rosenthal model [15]. This analytical solution provides the 3D thermal field for a moving heating source by considering thermal conductivity only. The temperature is given by:

$$T - T_0 = \frac{q}{2\pi k R} e^{\frac{v\rho c}{2k}(x-R)} \quad (5)$$

with T_0 being the room temperature, $R = \sqrt{x^2 + y^2}$ the radius from the laser spot, q the effective power, k the thermal conductivity, v the laser speed, and ρc the product of density and the heat capacity. It can be reformulated with reduced parameters:

$$T = C + \frac{A}{R} e^{B(x-R)} \quad (6)$$

with $C = T_0$, $A = q/2\pi k$ and $B = v\rho c/2k$. The parameter identification of A, B, and C from the thermography experiments was performed by using the optimization function SciPy in Python and the minimization of the square error with the L-BFGS-B method. The resulting parameters for pure 316L are given in Figure 6. The overall magnitude of the thermal field was fitted correctly. However, the Rosenthal model failed to predict the sharp increase of the thermal field along the x-axis for y = 0. This means that a model for only thermal conduction is unsuitable for predicting the experimental thermal field. There are two possible reasons for this. First, the latent heat of solidification was neglected and the solidification of the seam is exothermic and results in an increase in the temperature compared to the Rosenthal model. On this basis, the specific thermal properties of the powder were neglected in the Rosenthal model: the powder has a very low conductivity and acts as an insulator, but the seam is a bulk material with a higher conductivity. Therefore, the temperature increased on the axis y = 0 because of a faster diffusion of heat from the spot to the seam. The observation of the variation of the parameters A and B for the three composition is illustrated in Figure 7.

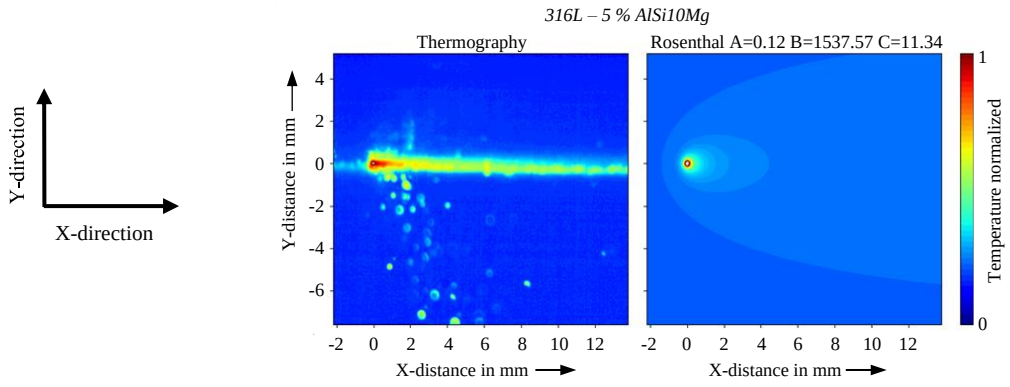

Figure 6: On the left, experimental thermographic images of the surface of the powder bed; on the right, the thermal field predicted by the Rosenthal model for the alloy 316L.

As indicated in Equation 6, the increase of *A* in Figure 7 was associated with an increase of the effective power *q*, or a decrease of the thermal conductivity *k*. The increase of *B* was associated with an increase of the specific heat capacity or a decrease of the thermal conductivity. According to literature, the addition of 1 % aluminum in α-Fe triggers a decrease of 30 % of the thermal conductivity [13]. If we assume the same variation for the 316L alloy, it would explain only half that increase of the parameter *B* when 1 % aluminum is added. Therefore, the thermal conductivity is probably not the only parameter affected by the composition change, and other factors have to be considered as well. Aluminum may for instance affect the emissivity and the heat capacity of the blended powder, resulting in the additional variation of *A* and *B*. Future investigations will be conducted to determine the exact contribution of the composition change to the heat diffusion in the built part and in the powder bed.

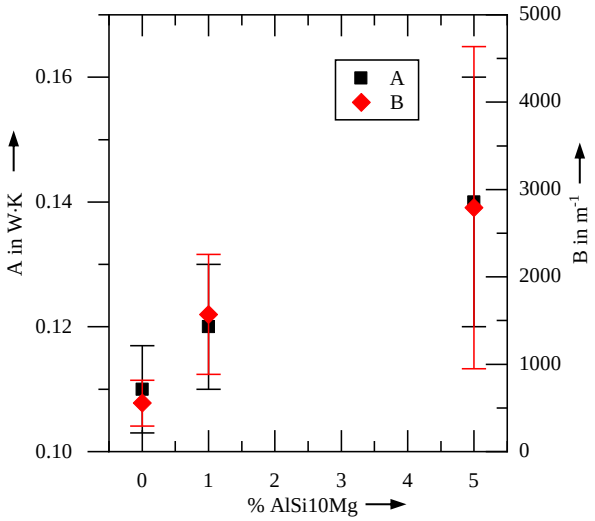

Figure 7: Variation of the parameters A and B according to Equation 6 with the addition of the aluminum additive.

Microstructure characterization

The phase stability of the three tested compositions was calculated via a computer aided thermodynamic study (Thermo-Calc). The phase diagram of Figure 8 predicts the phase formation upon solidification. According to Figure 8, the alloy with 1 % aluminum presents a main FCC phase and a very small percentage of BCC. However, in the alloy with 5 % aluminum, the major phase formed upon solidification is the BCC phase. To verify this and to correlate it with the solidification range, a simulation of the solidification was done using the Scheil-Gulliver model. As depicted in Figure 9, the melting range is not significantly affected by the addition of aluminum powder despite the significant

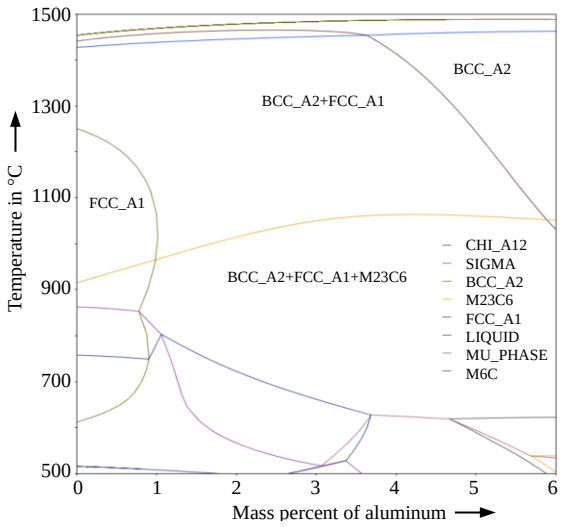

Figure 8: Phase diagram predicted by the Thermo-Calc software for 316L with the addition of aluminum.

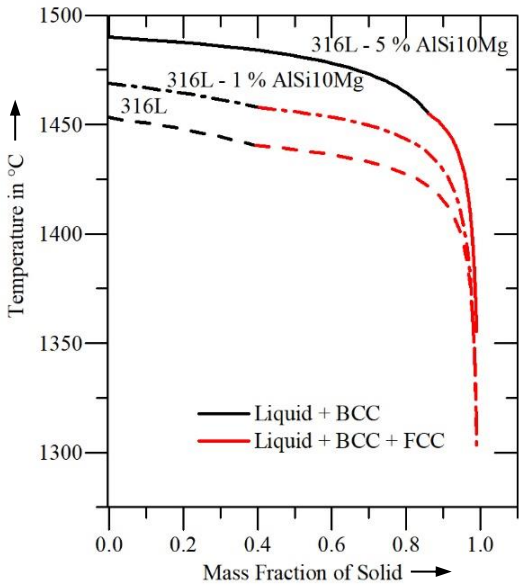

Figure 9: Evolution of the mass fraction of solidified material for the BCC (black line) and BCC+FCC phase (red line) calculated by the Scheil-Gulliver model.

difference in the melting points of the 316L with 5 % aluminum and the raw 316L powder.

The specimens of the LBM process that were used for thermographic imaging, served subsequently for microstructure characterization. The occurrence of phases was determined by XRD. The diagram is illustrated in Figure 10 for the three compositions. The specimens with 0 % and 1 % of additive showed peaks at 2θ = 51°,

59.5°, 89.4° and 111°, corresponding to the FCC austenite. The specimen with 5 % additive showed peaks at 52.1°, 76.9° and 99° corresponding to the BCC ferrite. The amplitude of the peaks was unusual: The FCC (111) peak usually has a maximal amplitude; however, the specimen exhibited a larger amplitude for the FCC (220) peak. Therefore, a severe texture of the material was present after solidification.

The phase identification was confirmed via EBSD. Figure 11 illustrates phase maps for FCC austenite (blue) and BCC ferrite (red). The specimen without additive was constituted of FCC phase only, with columnar grains oriented along the building direction. The Inverse Pole Figure (IPF) map showed a predominance of specific crystallographic orientations, suggesting a severe texture. After the addition of 1 % AlSi10Mg, the material remained mostly FCC, in agreement with the XRD diagram. However, blocks of BCC phase were visible, with a fraction low enough to remain undetected by XRD. The BCC block visible in Figure 11 b) is curved and is reminiscent of the typical geometry of the melt pool of the LBM process. For 5 % AlSi10Mg, the FCC phase was entirely replaced by BCC ferrite.

The IPF map shows a typical microstructure for the LBM process, with grains oriented along the building axis, but there is a lower fraction of columnar grains. The texture seems to be less marked as well. Figure 9 suggests that for a high content of aluminum, solidification was directly due to the formation of δ ferrite instead

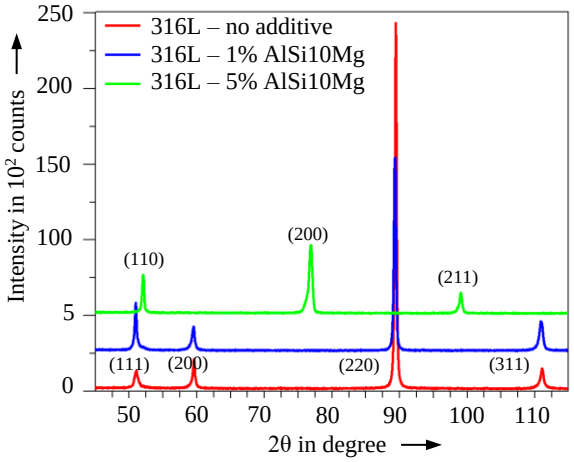

Figure 10: XRD diffractogram for 316L – no additive (red), 316L – 1 % AlSi10Mg (blue) and 316L – 5 % AlSi10Mg (green).

of austenite, and this may explain the sudden change of the microstructure for this composition.

The material with 5 % additive aluminum also exhibited a very large fraction of cracks. A crack is visible in Figure 11 c), and a complex network of cracks is evident in Figure 12 b). It indicates that the change in the solidification path severely increased the emergence of thermal distortions and residual stresses, resulting in the cracking of the material during the solidification. Further investigations are needed to understand this

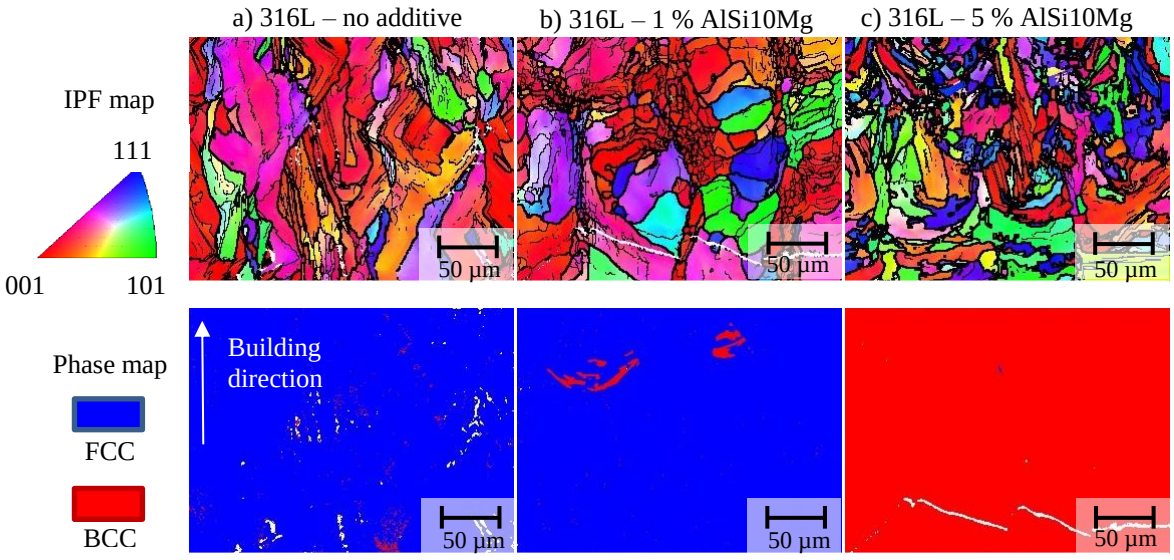

Figure 11:Above: Inverse Pole Figure (IPF) maps for a) 316L alloy, b) 316L – 1 % AlSi10Mg, c) 316L – 5 % AlSi10Mg; below: phase maps with FCC in blue and BCC in red.

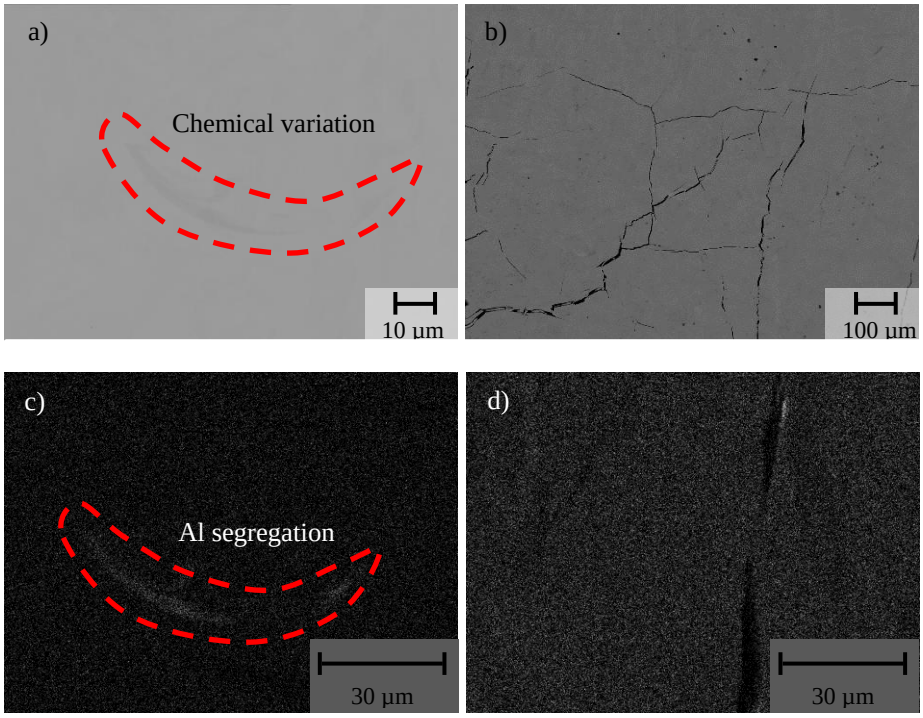

Figure 12: Electron Backscatter Diffraction (BSE) image of a) 316L – 1 % AlSi10Mg and b) 316L – 5 % AlSi10Mg; and EDX mapping of aluminum for c) 316L – 1 % AlSi10Mg and d) 316L – 5 % AlSi10Mg.

phenomenon. The laser melting of powder blends may result in chemical heterogeneities and inclusions [11]. To verify the existence of chemical fluctuations, BSE imaging was performed to detect variations of the chemical contrast (see Figure 12 a) and b)). A variation in contrast is visible in Figure 12 a). A domain with a lower brightness is discernible and it is possibly associated with a possible higher concentration of light elements. To confirm this observation, EDX mapping was conducted for the main elements of the material. The mapping showed no heterogeneities for the main elements (Fe, Cr, Ni, Mo), but a variation of the concentration of aluminum was detected at this location. Figure 12 c) illustrates the variation of the aluminum concentration by EDX mapping. The heterogeneity has a curved shape, and is reminiscent of the shape of the LBM melt pool. Consequently, it was assumed that the curved inclusions of aluminum can be associated with the emergence of curved domains of BCC phase in Figure 11 b). According to the Scheil-Gulliver model, solidification starts by the formation of the BCC phase. Therefore, a higher concentration of aluminum is expected in the primarily formed BCC phase, because aluminum is a BCC stabilizer. In the LBM process, solidification proceeds from the bottom of the melt pool to the top, with growth in the direction of the thermal gradient. Consequently, the formation of solid BCC started at the bottom of the melt pool and a higher concentration of aluminum formed in this region. Heterogeneities were more severely marked for 1 % additive, because the BCC growth occurred only at the very early stage of solidification. This resulted in aluminum-rich BCC blocks visible in Figures 11 b) and Figure 12 c). For a larger concentration of aluminum, the solidification proceeded with BCC phase only, and aluminum was homogeneously included in this phase.

Discussion

The investigated key characteristics (cooling factor, number of spatters and phase formation) have a major influence on the resulting part properties such as mechanical strength, dimensional accuracy and surface roughness. Both the results gained from thermographic imaging and the microstructure analysis indicate a high dependency on the amount of additives. Regarding the occurrence of the BCC phase, the theoretical predictions of the Scheil-Gulliver model showed consistency with the experimental results of the XRD analysis of the specimens. This proves that additives are able to influence the key characteristics and thus the final part properties in AM. Nevertheless, a correlation between the cooling factor and the microstructure formation could not be achieved due to the lack of a statistically validated data base. For further studies, experimental in-

vestigations with a larger scope are proposed. Therefore, the suitable range for the amount of additives must be identified with a narrow gradation of the additive content. In addition, the impact of further alloying components such as Si or Mg must be excluded by conducting studies with pure aluminum.

Conclusions

316L powder was modified by adding AlSi10Mg powder in a similar particle size distribution. The influence of the additive content on the melt pool was investigated using high-speed thermographic imaging. Subsequently, a thorough microstructure analysis was conducted. The findings of this paper are to be summarized as follows:

- A rotatory cylindrical container is suitable for the preparation of a homogeneous powder blend without pre-sintering the particles.
- Thermographic investigations of the melt pool showed that the cooling factor of the melted tracks depends on the additive content.
- According to the Rosenthal model, the thermal conductivity is probably not the only parameter that is affected by the composition change.
- Microstructure analysis demonstrated that a higher amount of AlSi10Mg increases the formation of the BCC phase.
- Specimens from the powder with 5 % additives exhibited a larger fraction of cracks compared to pure 316L powder.

To conclude, additives have a significant influence on the melt pool temperature field and the microstructure of manufactured components. Hence, identifying the suitable amount of additives is crucial for further studies.

Acknowledgement

The authors express their sincere gratitude to the German-French Academy for the Industry of the Future founded by the Institut Mines-Télécom (IMT) and the Technical University of Munich (TUM) for financially supporting the research on the presented topic within the research project ADAM. Furthermore, the authors would like to thank Katia Rodewald from the Wacker-Chair of Macromolecular Chemistry of the Technical University of Munich.

References

[1] H. Krauss, M. F. Zaeh (2013) Physics Procedia 41, pp. 815-822, 10.1016/j.phpro.2013.03.153

[2] S. Gorsse, C. Hutchinson, M. Gouné, R. Banerjee (2017) Science and Technology of Advanced Materials 18, pp. 584-610, 10.1080/14686996.2017.1361305

[3] T. Mukherjee, J.S. Zuback, A. De, T. Debroy (2016) Scientific Reports 6, p. 19717, 10.1038/srep19717

[4] T. Voisin, N.P. Calta, S.A. Khairallah, J.B. Forien, L. Balogh, R.W. Cunningham, A.D. Rollett, Y. Morris Wang (2018) Materials & Design 158, pp. 113-126, 10.1016/j.matdes.2018.08.004

[5] R. Cunningham, A. Nicolas, J. Madsen, E. Fodran, E. Anagnostou, M.D. Sangid, A.D. Rollett (2017) Materials Research Letters 5, pp. 516-525, 10.1080/21663831.2017.1340911

[6] M. Benedetti, V. Fontanari, M. Bandini, F. Zanini, S (2018) Carmignato, International Journal of Fatigue 107, pp. 96–109, 10.1016/j.ijfatigue.2017.10

[7] C. Zhao, K. Fezzaa, R. Cunningham, H. Wen, F. Carlo, L. Chen, A.D. Rollett, T. Sun (2017) Scientific Reports 7, p. 3602, 10.1038/s41598-017-03761-2

[8] A.A. Martin, N.P. Calta, J.A. Hammons, S.A. Khairallah, M.H. Nielsen, R.M. Shuttlesworth, N. Sinclair, M.J. Matthews, J.R. Jeffries, T.M. Willey, J.R.I. Lee (2019) Materials Today Advances, p. 100002, 10.1016/j.mtadv.2019.01.001

[9] Y. Brif, M. Thomas, I. Todd (2015) Scripta Materialia 99, pp. 93-96, 10.1016/j.scriptamat.2014.11.037

[10] C. Haase, F. Tang, M.B. Wilms, A. Weisheit, B. Hallstedt (2017) Materials Science & Engineering A 688 pp. 180–189, 10.1016/j.msea.2017.01.099

[11] M. Fischer, D. Joguet, G. Robin, L.Peltier, P.Laheurte (2016) Materials Science and Engineering C 62, pp. 852-859, 10.1016/j.msec.2016.02.033

[12] M. Martin, S. Weber, W. Theisen, T. Michler, J. Naumann (2013) Journal of Hydrogen Energy 38, pp. 5989-6001., 10.1016/j.ijhydene.2013.02.127

[13] B.J. Keene (1993) International Materials Reviews 38, pp. 157-192, 10.1179/imr.1993.38.4.157

[14] Y. Terada, K. Ohkubo, T. Mohri, T. Suzuki (2002) ISIJ International 42, pp. 322–324, 10.2355/isijinternational.42.322

[15] D. Rosenthal (1946) Transactions ASME 43, pp. 849-866

Meet the Authors

Andreas Wimmer is a research associate and doctoral candidate at the Institute for Machine Tools and Industrial Management (*iwb*) at the Technical University of Munich (TUM). He studied physics at the Ludwig-Maximilians University of Munich with a focus on solid state physics. His research is in the field of Additive Manufacturing (AM) with a special focus on Laser Beam Melting (LBM). Together with other groups of the Technical University of Munich he aims for a better process understanding.

Cara G. Kolb is a research associate and doctoral candidate at the *iwb*. She studied mechanical engineering with a focus on thermodynamics and management at the TUM. Her research is in the field of AM with a special focus on LBM, enabling the process to fabricate industry-relevant components of a high dimensional accuracy and surface quality.

Mariam Assi studied mechanical engineering at the Lebanese University, with a focus on construction and Energetics. She got her Master's degree in Materials Science and Engineering from Ecole des Mines Saint-Etienne, France. She is currently pursuing her PhD studies at Laboratoire Georges Friedel, EMSE. In her thesis, she is focusing on designing new alloys for the process of AM, in specific LBM, which requires a full understanding of the process and its specifications.

Julien Favre is Assistant Professor in Mines Saint-Etienne in France, and he dedicates his research on the alloy design for additive manufacturing. His major is Materials Science, and his expertise is on the materials characterization, metallurgy, and the physical modeling. In a previous position, he worked in LEM3 laboratory on the development of architectured lattice materials by additive manufacturing. He aims at developing new designs of materials for better specific properties.

Andreas Bachmann is the head of the Additive Manufacturing group and doctoral candidate at the *iwb*. He studied mechanical engineering with a focus on fundamentals in engineering sciences, control theory, and production engineering at the TUM. His research is in the field of Friction Stir Welding as well as in AM with a special focus on LBM, WAAM, and Binder Jetting.

Anna Fraczkiewicz has obtained her M. Sc. and engineer diploma in Warsaw University of Technology (Poland) and her PhD in Ecole des Mines de Saint-Etienne (France). She is professor in Ecole des Mines with an expertise field dealing with microstructural optimisation of metallic alloys (steels, intermetallics, Ni-based alloys) and the design of new austenitic HEAs (high entropy alloys).

Michael F. Zaeh is the head of the Institute for Machine Tools and Industrial Management as well as full professor for Machine Tools and Manufacturing Technologies at the TUM. His research focuses on machine tools, joining and cutting technologies, additive manufacturing technologies and cognitive systems for machine tools.